Applied Catalysis B: Environmental 206 (2017) 65–73

Contents lists available at ScienceDirect

Applied Catalysis B: Environmental

journal homepage: www.elsevier.com/locate/apcatb

A facile sol-gel synthesis of highly active nano α-aluminum fluoride catalyst for dehydrofluorination of hydrofluorocarbons

Wei Mao[a,b], Yanbo Bai[a,b], Bo Wang[a,b], Wei Wang[a,b], Hui Ma[a,b], Yue Qin[a,b], Chen Li[a,b], Jian Lu[a,b,*], Zhongwen Liu[c,**]

[a] State Key Laboratory of Fluorine & Nitrogen Chemicals, Xi'an, Shaanxi 710065, China
[b] Xi'an Modern Chemistry Research Institute, Xi'an, Shaanxi 710065, China
[c] School of Chemistry & Chemical Engineering, Shaanxi Normal University, Xi'an 710119, China

ARTICLE INFO

Article history:
Received 19 August 2016
Received in revised form
25 December 2016
Accepted 27 December 2016
Available online 27 December 2016

Keywords:
Aluminum fluoride
Dehydrofluorination
Sol-gel
Heterogeneous catalysis
1,1,1,2-tetrafluoroethane

ABSTRACT

Nano α-aluminum fluorides with high surface area were synthesized by a simple ethylene glycol mediated sol–gel technique using dilute aq. HF as the F source, and their performances were investigated for gas-phase dehydrofluorination of 1,1,1,2-tetrafluoroethane at relatively low reaction temperature (400 °C). Aluminum precursor was crucial for the phase composition, textural and acidic properties of the resulting fluoride. Commercially low-cost and available inorganic Al was firstly used as precursor for synthesis of aluminum fluorides via the sol–gel route, and the as-prepared α-AlF_3 possessed high surface area (up to 170 $m^2 g^{-1}$) and strong surface acidities even after thermal treatment of 400 °C. The presence of sulfate ions suppressed the crystallization of aluminum fluoride during calcination when $Al_2(SO_4)_3$ was used as precursor, leading to an amorphous phase for as-prepared AlF_3. Aluminum fluorides with β and pyrochlore phase were prepared using aluminum isopropoxide and aluminum diacetate hydroxide, respectively, as precursors. Based on the results of IR, XRD and element analysis, it is concluded that the formation of Al-glycolates during the sol–gel process can effectively reduce the hydrolysis of precursor and suppress particle agglomeration, thus leading to dominant formation of *nano* aluminum fluorides. The residual O derived from minor hydrolysis can resist sintering under high-temperature treatment, which is a key factor to improve the thermostability of as-prepared aluminum fluoride. Due to their large Lewis acidic amounts, the α-AlF_3 derived from AlOOH and Al_2O_3 exhibited remarkably high catalytic activity with CF_3CH_2F conversion of 24%–28% and CF_2=CHF selectivity above 98%, which were far higher than that of AlF_3 prepared by traditional methods.

1. Introduction

As alternatives of chlorofluorocarbons (CFCs), hydrofluorocarbons (HFCs) such as 1,1,1,2-tetrafluoroethane (HFC-134a) are widely used as refrigerants, foaming agents and cleaning agents in modern society. However, most of HFCs have high global warming potential (GWP), which can lead to climate change as potent greenhouse gases [1]. As a consequence, the Kyoto Protocol established the phasing out of HFCs, and any refrigerant with a GWP over 150 has been forbidden in the air conditioning systems of new car by the EU since 2011 [2]. Thus, it is very urgent to decompose or transform HFCs to other eco-friendly and valuable chemical compounds. Gas-phase dehydrofluorination of HFCs to hydrofluoroolefins (HFOs) is obviously an ideal strategy to resolve above issue. The high reactivity of C=C double bond gives HFOs short atmospheric lifetimes and low GWP values, which are considered as the new environmental benign alternatives to HFCs and as important F-containing monomers [3–5].

Gas-phase dehydrofluorination of HFCs is typically an endothermic reaction due to high strength of C–F bond both in thermodynamics and kinetics [4,6], where high temperature is necessary for achieving acceptable conversion. Thus, highly active catalyst is desirable in this reaction to improve the yield of fluorinated olefins. In catalytic reaction involving HF and elevated-temperature conditions, metal fluorides and oxide-fluorides stand out among numerous catalytic materials owing to their irreplaceable stability under such a corrosive atmosphere. Thereinto, aluminum fluorides are one class of well-known catalysts for

* Corresponding author at: State Key Laboratory of Fluorine & Nitrogen Chemicals, Xi'an, Shaanxi 710065, China.
** Corresponding author.
E-mail addresses: lujian204@gmail.com (J. Lu), zwliu@snnu.edu.cn (Z. Liu).

http://dx.doi.org/10.1016/j.apcatb.2016.12.064
0926-3373/

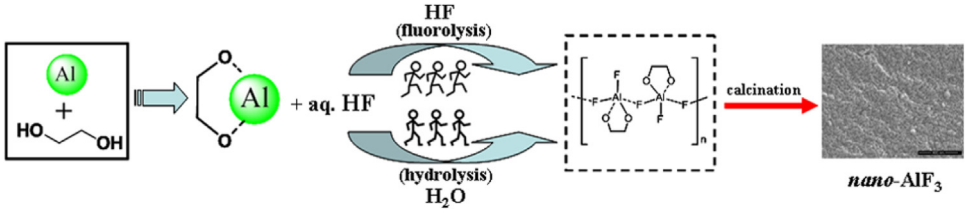

Scheme 1. Ethylene glycol mediated sol–gel (EGSG) process for synthesis of nano-aluminum fluorides.

synthesis of HFCs and their transformation [7,8]. For HFC dehydrofluorination, it is recognized that catalytic activity is related to the surface acidity of catalyst [4,9], and the latter is highly dependent on the specific surface area and nanostructure of aluminum fluoride [10,11] and hence the method of preparation. Unfortunately, due to high lattice energy of metal fluorides, aluminum fluorides conventionally prepared by gas-phase fluorination or precipitation give very low specific surface area (10–60 $m^2\,g^{-1}$) with weak acidity [4,10], resulting in a low activity in dehydrofluorination of 1,1,1,2-tetrafluoroethane (HFC-134a) at 400 °C (conv. < 10%) [4]. Therefore, the development of *nano*-aluminum fluoride catalyst with large specific surface area becomes a significant topic in heterogeneous catalysis.

Over past decades, to prepare aluminum fluorides with high specific surface area (>100 $m^2\,g^{-1}$) (denoted as HS-AlF_3), a variety of elaborate synthetic approaches have been developed, e.g., fluorolytic sol–gel route [7], plasma-etching fluorination [12], oxidative decomposition [8], carbon-template fluorination [13], microwave hydrothermal process [14], etc. Noteworthy, either multistep procedures or severe preparation conditions and costly alkoxides are prerequisite to achieve high specific surface area in above methods. More importantly, most of prepared HS-AlF_3 are amorphous phase which are not stable at elevated temperature (>350 °C), leading to a collapse of the porous structure and sintering accompanied by dramatic decrease of specific surface area [10,13,15]. Thus, above aluminum fluorides are not suitable as catalysts for some reactions requiring high temperatures, such as dehydrofluorination of HFC-134a. The thermodynamic stable phase is α-AlF_3, moreover, recent theoretical and experimental studies have confirmed that nano-sized α-AlF_3 possesses strong acidity and catalytic activity [16,17]. Nevertheless, few insights have been gained so far on the synthesis of α-AlF_3 with high specific surface area (HS-α-AlF_3). Only Medina et al. reported the synthesis of HS-α-AlF_3 (S_{BET} = 123 $m^2\,g^{-1}$) by thermal decomposition of β-$AlF_3{\cdot}3H_2O$ under an argon-flowing atmosphere at 350 °C [18]. Up to now, to our knowledge, no other convenient strategy is reported for preparation of HS-α-AlF_3. Thus, for industrial applications, it remains very essential but challenging to develop a facile synthetic approach for HS-α-AlF_3 with strong acidity and excellent thermostability.

In this work, we introduced a novel synthesis of *nano* α-aluminum fluorides with high specific surface area via a facile sol–gel process, and evaluated the catalytic activities of as-prepared aluminum fluorides on dehydrofluorination of HFC-134a. Ethylene glycol (EG), known for its strong chelating ability with metal ions [19–21], was used as solvent to limit the particle growth of fluorides and to prevent the formation of precipitates, leading to a sol–gel process. Commercially low-cost and available inorganic Al including boehmite, oxides and inorganic salt hydrates were firstly used as precursors for synthesis of aluminum fluorides via the sol–gel route. A dilute aqueous hydrofluoric acid (40 wt.%) was used as F sources. Afterward, HS-α-AlF_3 (120–170 $m^2\,g^{-1}$) was achieved even after a high temperature calcination (400 °C) using above aluminum sources as precursors. In addition, by altering aluminum precursors, aluminum fluorides with amorphous, β and pyrochlore phase were also obtained via the proposed method. The whole process is illustrated in Scheme 1. Based on extensive characterization, the effects of aluminum precursors on the final aluminum fluorides were discussed. Several characterization techniques (XRD, IR, SEM/EDX, TEM and element analysis) were used to elucidate the excellent stability of resulting material towards elevated temperature. The FT-IR spectra of pyridine adsorption, NH_3-TPD and BET studies were investigated to explain different catalytic behaviours.

2. Experimental

2.1. Chemical materials

Commercially available $Al(NO_3)_3{\cdot}9H_2O$ (denoted as ANO), $AlCl_3{\cdot}6H_2O$ (denoted as ACl), $Al_2(SO_4)_3{\cdot}18H_2O$ (denoted as ASO), aluminum isopropoxide ($Al(OiPr)_3$) (denoted as AIP), aluminum diacetate hydroxide ($C_4H_7AlO_5$) (denoted as ADH), and ethylene glycol (denoted as EG) were purchased from Sinopharm Chemical Reagent Co., Ltd. The γ-Al_2O_3 (denoted as AO) and boehmite (AlOOH) (denoted as AOH) were purchased from Zibo Reagent Co., ShanDong, China. All the chemicals used in the experiment were analytical grade and used without any further purification.

2.2. Preparation of HS-α-AlF_3

The ANO, ACl, AO and AOH, respectively, were used as precursors for preparation of HS-α-AlF_3. The general procedure via the ethylene glycol mediated sol–gel (EGSG) process is as follows: (I) the required amount of Al-precursor was dissolved in ethylene glycol (50 mL) at 50 °C (Al concentration = 1.0 M) in a PTFE beaker, but a suspension was present using AOH and AO, respectively, as precursor. (II) The aqueous hydrofluoric acid (40 wt.%) was added to above solution in a stoichiometric amount (1:3 molar ratio for Al/F) under rigorous stirring for 6 h; then, a transparent and colourless sol was obtained (a light yellow for the ACl–derived sol). (III) The obtained sol was aged at 90 °C for 1 day, subsequently dried at 110 °C for 1 day. The yellow gel powders were obtained using ANO as the precursor, while other gels were white. (IV) The HS-α-AlF_3 was achieved by calcination of different gels under air atmosphere at 400 °C for 4 h with a ramping rate of 2 °C min^{-1}. The obtained gels and aluminum fluorides were designated as gel-x and AlF_3-x, respectively, where the x indicated the abbreviation of precursor.

2.3. Preparation of AlF_3 with amorphous, β and pyrochlore phase

The ASO was used as precursor for preparation of amorphous AlF_3. The aluminum fluorides with β and pyrochlore phase were prepared using ADH and AIP, respectively, as precursors. These aluminum fluorides were prepared using the same procedures described for synthesis of HS-α-AlF_3 in the section of *Preparation of HS-α-AlF_3*. For comparison, aluminum fluoride (denoted as AlF_3-EtOH) was also prepared using ethanol instead of EG as the solvent with ANO as the precursor under similar conditions.

2.4. Catalyst characterization

XRD patterns of the prepared samples were collected with an Empyrean, PANalytical X-ray diffractometer (Cu Kα, λ = 0.15418 nm). The pattern for the structure refinement was taken in a 2θ range of 5–90◦ with a step width of 0.02◦. The specific surface area of the sample was measured using nitrogen adsorption at 77 K and the Brunauer–Emmett–Teller (BET) method using a Micrometerics ASAP2020 system. All samples were degassed at 250 °C in vacuum for 8 h. Pore size distribution was determined by the Barret–Joyner–Halenda (BJH) method, applied to the desorption branch of the isotherm. The analysis of fluoride was carried out using a fluoride sensitive electrode after conversion of the solids with Na_2O_2/NaOH into a soluble form. The EDTA titration method was used to determine the Al contents of prepared fluorides after removal of fluorine from the soluble sample. The fluoride was removed by boiling the soluble sample for 1 min after the addition of boric acid. The total carbon and oxygen contents were determined using an elemental analyzer (Elementar Vario III).

The morphology of prepared AlF_3 was observed using a scanning electron microscope (SEM) (FEI Quanta 600FEG) operating on 20 kV. To determine the component in the sample along the surface section, the signals of surface elements were detected by the Energy-Dispersive X-ray spectroscopy (EDX) (Oxford INCA Energy IE350) mapping method. The particle size and morphology of the samples were also observed using a transmission electron microscope (TEM) (FEI Tecnai G2 F20) operating on 200 kV.

The temperature-programmed desorption of ammonia (NH_3-TPD) measurement was carried on an AutoChem II 2920 instrument (Micromeritics, USA) for comparing the acidity of various samples. Prior to NH_3-TPD studies, a sample of 100 mg was first pretreated in pure He at 450 °C for 60 min, then cooled to 110 °C and saturated at this temperature with anhydrous ammonia gas (10% in He) for 30 min. Weakly adsorbed NH_3 was eliminated by treatment under He at the same temperature for 60 min. The NH_3-TPD profile was recorded with a thermal conductivity detector with a heating rate of 10 °C min^{-1} from 110 to 450 °C in a He flow.

The infrared absorptions were studied adopting FT-IR spectrometer (Bruker Tensor27) for investigating the nature of bonding of prepared AlF_3, and the IR spectra of sample was recorded at room temperature on a thin disk (5 wt.% sample mixed with KBr) in the range of 4000–400 cm^{-1}. The evolution of the bonding of prepared gel during the thermal treatment was determined by means of an in situ FT-IR spectroscopy (Nicolet Nexus870). All the samples were heated under static air. After activation at 350 °C for 1 h, the Lewis and Brønsted acidities of the material were studied by an IR spectroscopy (PerkinElmer FT-IR Frontier), with adsorbed pyridine as a spectroscopic probe and a self-supported wafer of sample. Introduction of pyridine was performed at room temperature for 0.5 h and then evacuated under vacuum at 200 °C to remove physisorbed species. The Lewis acidity amount was calculated based on the intensity of ~1455 cm^{-1} band, and the molar extinction coefficient used was 2.2 cm μmol^{-1}. The 95% confidence limits were estimated at ±15%.

2.5. Catalytic reaction

Catalytic dehydrofluorination of HFC-134a was performed in a fixed bed stainless steel reactor (1 cm inner diameter) at atmospheric pressure. The reactor was heated by a tube furnace, and mass flow controllers (Sevenstar, D-07) were used to regulate the flow of gases to the reactor. The catalyst (5 mL) was pretreated in N_2 flow at 400 °C for 30 min before reaction, then the reaction temperature was maintained at 400 °C. The reactant was a mixture of HFC-134a (5.7 mL min^{-1}) and N_2 (50.9 mL min^{-1}). HFC-134a (99.9%) was provided by Xi'an Modern Chemistry Research Institute. Before reaction, the material was preheated in a vaporizer at 300 °C. After reaction the product gas was passed through a KOH solution to trap acid gases, then analyzed by a gas chromatograph (SICT GC-2000III) equipped with a flame ionization detector (FID) and a GS-GASPRO capillary column (60 m × 0.32 mm). The conversion of HFC-134a and selectivity of trifluoroethylene (CF_2=CHF) were calculated as defined:

$$\text{HFC-134a conversion} = \text{HFC-134a}_{in} - \text{HFC-134a}_{out}/\text{HFC-134a}_{in} \times 100\,\text{wt.\%}$$

$$\text{Trifluoroethylene selectivity} = \text{trifluoroethylene}_{out}/\text{HFC-134a}_{in} - \text{HFC-134a}_{out} \times 100\,\text{wt.\%}$$

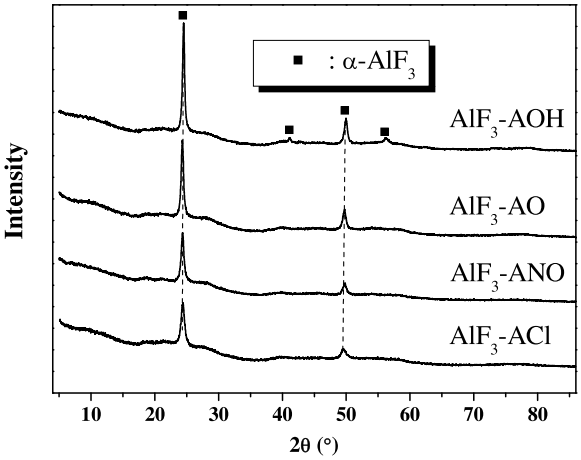

Fig 1. XRD patterns of α-AlF_3 derived from AO, AOH, ANO and ACl.

3. Results and discussion

3.1. Characterization of HS-α-AlF_3

3.1.1. Bulk structure and chemical composition

The X-ray diffraction (XRD) pattern (Fig. 1) reveals that AlF_3-AOH had diffraction peaks at 24.4°, 41.1°, 49.8° and 56.2°, which can be ascribed to the α-AlF_3 phase (JCPDS-80-1007) [16]. Despite differences in Al precursors, similar diffraction peaks were observed in AlF_3 derived from AO, ANO and ACl. Moreover, no other crystalline oxide, hydroxide or hydroxide fluoride species were detected in these samples. However, considering the broad diffraction peaks with low intensity, the amorphous structure can be hardly excluded in these aluminum fluorides. Thus, the prepared AlF_3 derived from AO, ANO and ACl may be a mixture of α-AlF_3 and amorphous AlF_3. Due to different full width at half maxima (FWHM) of diffraction peaks, the notable difference for above samples was their crystallite sizes. On basis of the Scherrer equation, these α-AlF_3 samples exhibited crystallite sizes in the range of 13.1–23.5 nm (Table 1). Interestingly, the corresponding gels also displayed similar crystalline structures as the synthesized aluminum fluorides (Supporting Information, Fig. S1), while the phase of hydrated aluminum fluoride was firstly formed in the conventional precipitation using aqueous F source [22,23]. Above results suggest that the hydration of aluminum fluoride is suppressive in the EGSG process. To confirm the unique property of EG, similar synthetic procedures were performed in the ethanol solvent with ANO as the precursor. The obtained precipitate exhibited the phase of $AlF_3 \cdot 3H_2O$ (JCPDS-43-0436) (Fig. S2). Therefore, the aluminum fluorides seem to be formed directly from the Al^{3+} ion and F^- in the EG without the formation of aluminum fluoride hydrate.

Table 1
Elemental compositions and crystallite sizes of various α-AlF_3.

Sample	Al[a] (wt.%)	F[b] (wt.%)	O[c] (wt.%)	C[c] (wt.%)	F/Al mol. ratio	Crystallite sizes[d] (nm)
AlF_3-AOH	30.5	62.5	4.6	1.3	2.91	18.1
AlF_3-AO	32.1	61.4	4.6	1.9	2.72	25.4
AlF_3-ANO	32.1	59.9	5.6	2.4	2.65	22.3
AlF_3-ACl	32.0	60.7	5.4	1.8	2.70	10.7

[a] Al content was determined by EDTA titration.
[b] F content was estimated by titration.
[c] The O and C contents were analyzed by an elemental analyzer.
[d] Average crystal size estimated using Scherrer equation.

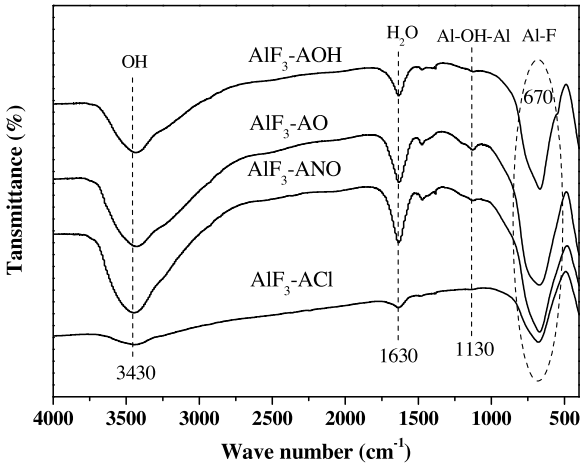

Fig. 2. FT-IR spectra of α-AlF_3 derived from AO, AOH, ANO and ACl.

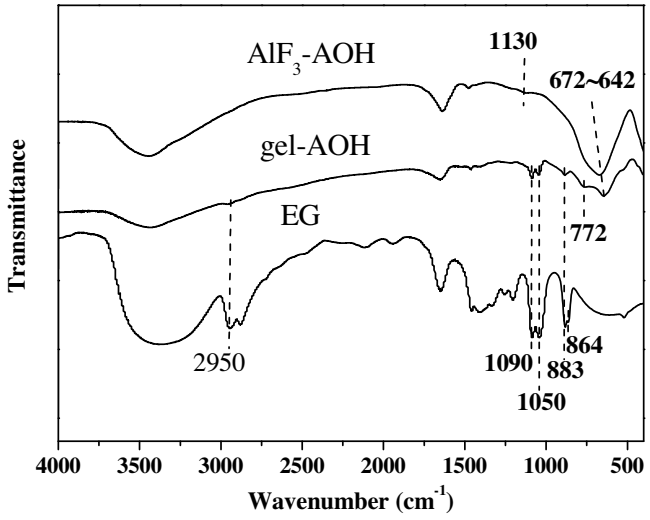

Fig. 3. FT-IR spectra of gel-AOH and AlF_3-AOH with EG.

The chemical compositions (Al, F, O and C) of prepared α-AlF_3 (Table 1) show that main components were Al (~32 wt.%) and F (~61 wt.%) for all the prepared α-AlF_3. For AlF_3-AOH, a little O (~4.6 wt.%) with trace amounts of C (~1.3 wt.%) was also detected, leading to a slightly low F/Al molar ratio (2.91). The oxygen content may be a result of minor hydrolysis of aluminum precursor during the EGSG process and surface hydration of solid exposed in ambient atmosphere. AlF_3-AO exhibited close chemical compositions to AlF_3-AOH, but its C content was a bit higher than the latter. The chemical compositions (Table S1) determined by energy dispersive X-ray spectroscopy (EDX) display similar results to the element analysis, where large amounts of Al and F with minor O can be observed in each α-AlF_3 sample. However, due to high relative error of EDX technique, its result is not totally consistent with the data obtained by the element analysis. Based on the results from Table 1, using inorganic salt hydrates (ANO and ACl) as precursors, the resulting AlF_3 possessed more O content than those using oxides as precursors, leading to relative low F/Al molar ratios (2.65–2.7). This indicates that although none of prepared aluminum fluorides were real pure AlF_3, the degree of fluorination was slight high in the aluminum fluorides derived from oxides.

To further determine the structure and composition, the FT-IR of prepared α-AlF_3 was also investigated (Fig. 2). FT-IR analysis showed an intense peak at 670 cm^{-1} in all samples, confirming the formation of Al–F bond in the prepared materials [10]. A very weak shoulder peak at 1130 cm^{-1} was also observed, which can be attributed to Al–OH–Al bending vibration [24], indicating the occurrence of small amount of hydrolysis. Above results coincided with the elemental analysis of various α-AlF_3 samples. Therefore, the IR spectra demonstrate the formation of crystalline and partially hydoxylated AlF_3.

To understand the formation of aluminum fluoride in the proposed sol–gel process, we then compared the FT-IR results of EG, gel-AOH and AlF_3-AOH (Fig. 3). The characteristic adsorption of EG (~2950, 1090, 1050 and 883 cm^{-1}, respectively) was observed in gel-AOH [25]. The C content of gel-AOH reached to 13.1 wt.%, also supporting the presence of EG in as-prepared dried gel. It should be noted that the CH_2 rocking vibration (883 cm^{-1}) and the C—C stretching vibration (864 cm^{-1}) of EG were merged into a single band at 883 cm^{-1} in gel-AOH, indicating the formation of a bidentate complex between Al and EG [25]. Furthermore, in comparison with EG, gel-AOH exhibited two new bands at 772 (Al—O stretching) and 642 cm^{-1} (Al—F stretching) [26], while the bending vibration of Al—OH—Al at ~1100 cm^{-1} was not visible. Whereas, in the traditional fluorolytic sol–gel method (AlP and aq. HF as raw materials, anhydrous methanol as solvent), the obtained gels of aluminum fluoride always show the characteristic IR absorption of Al—OH—Al bond due to partial hydrolysis of Al precursor [26,27], although fluorolysis is superior to hydrolysis both in thermodynamics and kinetics [7,28]. One rational explanation for above results is that the Al—O bond was mainly derived from the formed Al-glycolates which inhibited the hydrolysis in our EGSG. Interestingly, the IR absorption of Al—OH—Al bond was present in AlF_3-AOH, while the IR absorption of Al—O bond disappeared. We used in situ FT-IR to further investigate the evolution of gel-AOH during the calcination (Fig. S3). For temperature above 200 °C, the characteristic adsorptions of EG, water and band at ~770 cm^{-1} were not observed, while a weak peak at 1130 cm^{-1} was observed. This reveals that minor hydrolysis occurred when EG was removed from the as-prepared gel during the thermal treatment. These IR results explain the formation of aluminum fluoride during the EGSG process, supporting the conclusion shown in Scheme 1.

3.1.2. Texture and morphology

The N_2 sorption measurements (Fig. 4 and Table 2) reveal that all the fluorides presented high BET specific surface area

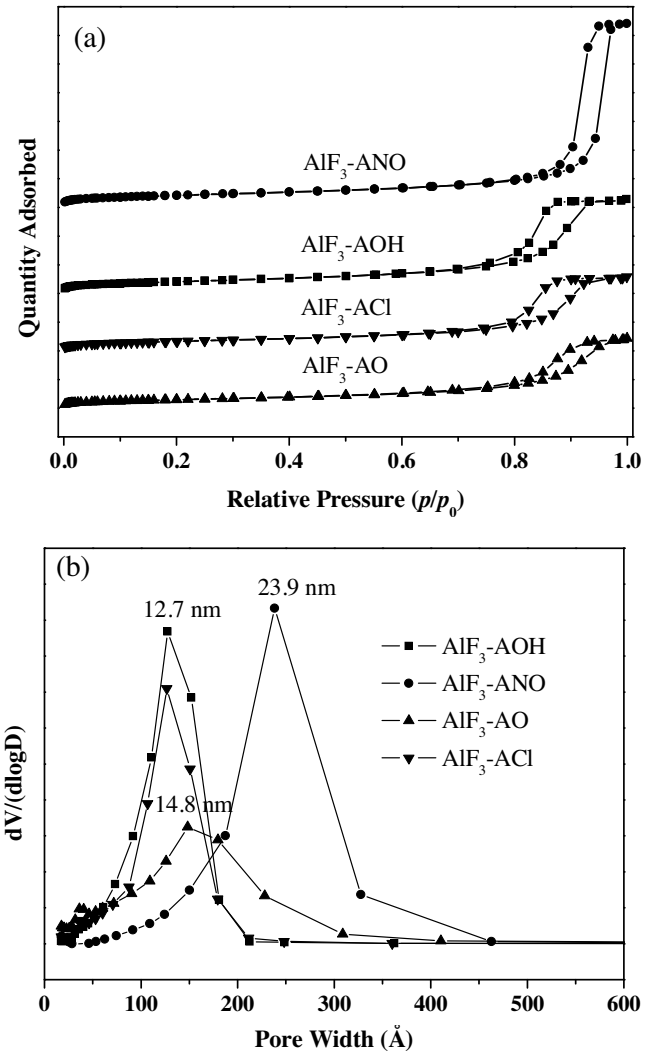

Fig. 4. N_2 sorption isotherms (a) and the distribution of pore sizes from the desorption branch of the isotherm (b) for AlF_3 derived from AO, AOH, ANO and ACl.

Table 2
Textural properties of as-prepared α-AlF_3.

Sample	Surface area ($m^2\ g^{-1}$)	Av. pore diameter (nm)	Pore volumed ($cm^3\ g^{-1}$)[a]
AlF_3-AOH	150	18.1	0.57
AlF_3-AO	120	25.4	0.42
AlF_3-ANO	170	22.3	1.11
AlF_3-ACl	134	10.7	0.45

[a] Pore volume is the total internal pore volume measured at $P/P_0 = 0.99$.

(120–170 $m^2\ g^{-1}$) with a type IV isotherm. Type H2 hysteresis loop at high P/P_0 (0.7–1.0) suggested the presence of large mesopores in all prepared α-AlF_3 materials, which can be formed by the agglomeration/aggregation of primary nanoparticles [29]. Furthermore, aluminum fluorides derived from inorganic salt hydrates displayed higher specific surface area than those derived from oxides. In particular, much high specific surface area of 170 $m^2\ g^{-1}$ was achieved in AlF_3-ANO. As gathered from results of elemental analysis, the large specific surface area may be attributed to higher O content in AlF_3-ANO than in other oxide precursors based-fluorides. Furthermore, Demourgues et al. have reported that the use of nitrate as precursor enabled the stabilization of the nanostructure of prepared AlF_3 [30]. Nevertheless, AlF_3-ACl had higher amount of oxygen in comparison with AlF_3-AOH despite a lower specific surface area. It is deduced that the substitution of OH groups by the Cl anion was not beneficial to stabilize to some extent the nanostructure of aluminum fluorides, resulting in a relative low specific surface area. The pore size distribution (Fig. 3b) exhibited a sharp peak centered among 12–24 nm for all the samples (calculated from the desorption branch of the nitrogen isotherm with the BJH method), which, together with the sorption isotherm results, suggested that the prepared α-AlF_3 samples were mesoporous materials. In addition, except AlF_3-AO, the specific surface areas obtained here exceeded those of α-AlF_3 (S_{BET} = 123 $m^2\ g^{-1}$) synthesized by calcination of β-$AlF_3{\cdot}3H_2O$ at low temperature (350 °C) [18]. These results confirm that HS-α-AlF_3 was accessible via our approach even after high temperature calcination (400 °C).

The morphologies of prepared HS-α-AlF_3 were examined by scanning electron microscopy (SEM) (Fig. S4) and transmission electron microscopy (TEM) (Fig. 5). The SEM images reveal that all the prepared aluminum fluorides were formed by the densely random accumulation of nano-particles. The TEM investigations reveal different morphologies for prepared samples. The image of AlF_3-AOH (Fig. 5a) showed the presence of nanorod-like structure with typical thicknesses around 5–10 nm. Moreover, the nanorods were highly interconnected and aggregated, leading to the formation of mesoporous voids, which agreed well with the N_2-sorption results. Note that the particle sizes obtained from TEM were smaller than those obtained from XRD. This can be ascribed to the fact that XRD reflects the crystalline particles, not the actual morphologies of materials. Furthermore, large particles are counted in the XRD, and numerous small particles are picked in the TEM. As shown in Fig. 5b, AlF_3-AO consisted of more aggregated nanorods (thickness 7–10 nm) than AlF_3-AOH. The image of AlF_3-ANO (Fig. 5c) revealed the structure of connected particles, and AlF_3-ANO possessed much high porosity which explained its largest specific surface area in the prepared HS-α-AlF_3 samples. For AlF_3-ACl, the solid consisted of agglomerates building from irregularly shaped nanoparticles. Such large specific surface area with mesoporous properties and good textural stability make the prepared HS-α-AlF_3 a promising catalyst or support, especially for high temperature reactions.

3.2. Characterization of AlF_3 with amorphous, β and pyrochlore phase

Another Al sources have been also investigated to prepare aluminum fluoride in the proposed method. Using ASO as precursor, amorphous phase dominated in the resulting AlF_3 (Fig. 6), although the distinct peak of α-AlF_3 can be detected. Using AlP as precursor, aluminum fluoride with pyrochlore framework (aluminum hydroxyfluoride, JCPDS-78-2260) was obtained in our method. Similar aluminum hydroxyfluoride was also achieved in the fluorolytic sol–gel method using the same Al precursor and F source [27]. Owing to high hydrolysis rate of alkoxides, competing hydrolysis became increasingly important when dilute aq. HF was used as the F sources [7]. The AlF_3 derived from ADH exhibited a β-AlF_3 phase (JCPDS-84-1672).

The EDX analysis (Table 3) showed that large amounts of O and S were present in AlF_3-ASO. The relative IR spectra (Fig. S5) also revealed the presence of SO_4^{2-}. Furthermore, the IR spectrum of AlF_3-ASO exhibited the characteristic adsorption of Al—F bond at 667 cm^{-1}, which was much broader than those observed in the other aluminum fluoride samples, indicating the domination of amorphous AlF_3 in AlF_3-ASO [10]. This result was consistent with the XRD result. Several papers have reported that impregnated sulfate ions can retard the crystallization of metal oxides during calcination [31]. Our results described here demonstrated that the residual sulfate ions can also retard the crystallization of aluminum fluoride at elevated temperature, resulting in an amorphous phase with the highest specific surface area of 190 $m^2\ g^{-1}$ among the pre-

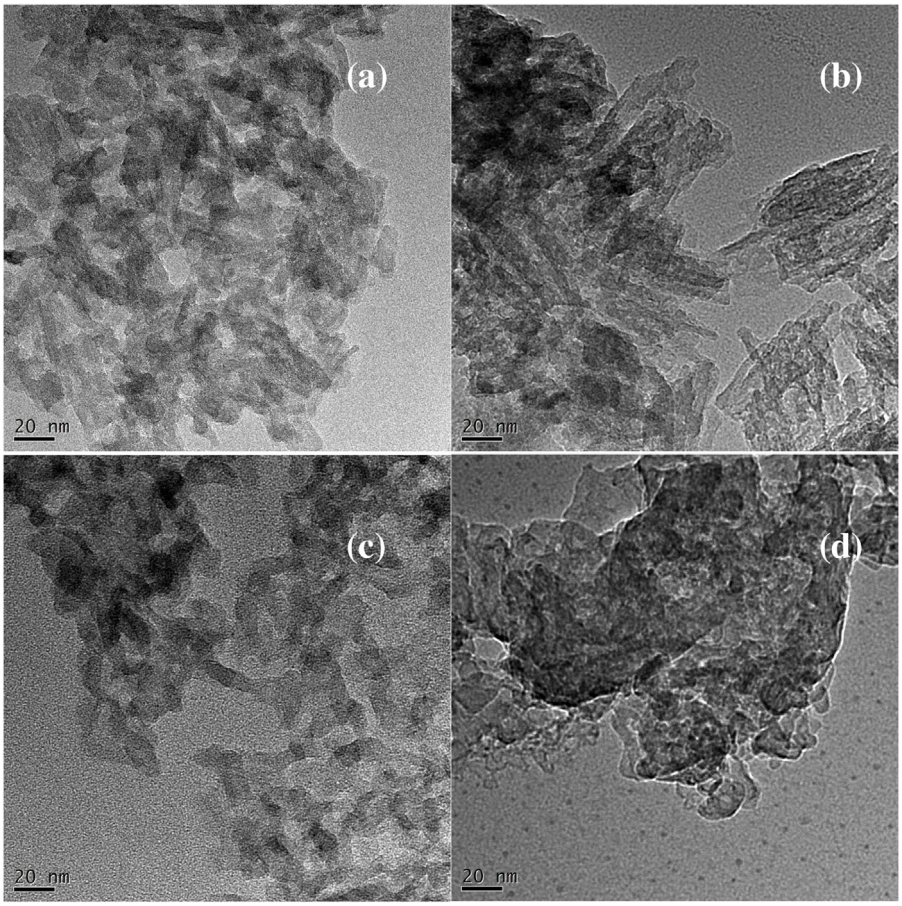

Fig. 5. TEM images of various HS-α-AlF_3. (a) AlF_3-AOH, (b) AlF_3-AO, (c) AlF_3-ANO and (d) AlF_3-ACl.

Table 3
Textural properties and elemental compositions of AlF_3 derived from ADH, AIP and ASO detected by EDX.

Sample	Surface area ($m^2\ g^{-1}$)	Pore volumed ($cm^3\ g^{-1}$)	Al (wt.%)	F (wt.%)	O (wt.%)	C (wt.%)	S (wt.%)
AlF_3-ADH	31	0.08	26.8	70.3	1.9	1	–
AlF_3-AIP	97	0.26	29	55.5	13.4	2.1	–
AlF_3-ASO	191	0.37	20	39.6	23.6	6.8	10

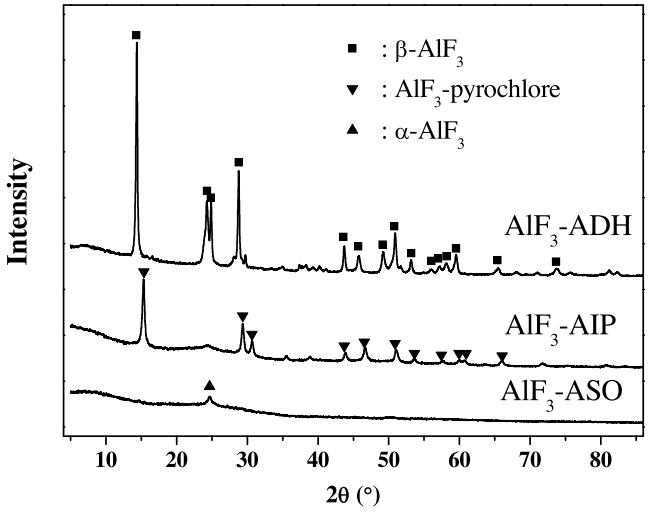

Fig. 6. XRD patterns of AlF_3 derived from ASO, AIP and ADH.

pared samples. For AlF_3-AIP, the O content increased to ~13.4 wt.%, which was in agreement with the XRD result. More importantly, the FT-IR results (Fig. S6) show that two absorption bands at 883 and 864 cm^{-1} assigned to EG were observed in gel-AIP, while the absorption of the Al—O bond derived from Al-glycolates was absent. This result suggests that the interaction between Al and EG was weaker using AIP as precursor than using AOH as precursor, leading to higher hydrolysis. Notably, AlF_3-AIP still had a relatively high specific surface area of 97 $m^2\ g^{-1}$ even after calcination of 400 °C. The specific surface area increased to 116 $m^2\ g^{-1}$ when calcination temperature decreased to 350 °C, which was close to those of aluminum hydroxyfluoride prepared under low temperatures by fluorolytic sol–gel method [27,28] or microwave hydrothermal method [14]. AlF_3-ADH showed a low specific surface area (31 $m^2\ g^{-1}$) like the common β-AlF_3. The Al and F accounted for 97.2 wt.% of AlF_3-ADH, while the O content was low (1.9 wt.%). In contrast, the O content reached to 4–24 wt.% in the prepared HS-α-AlF_3, AlF_3-AIP and AlF_3-ASO, which had large specific surface area. Accordingly, it is likely that the residual O was responsible for the stabilization of synthesized aluminum fluoride nanoparticles at elevated temperature.

The TEM image (Fig. 7a) of AlF_3-ASO exhibited an amorphous structure with high mesoporosity (pore diameter of 5–30 nm), which agreed well with the XRD and N_2-sorption results. The TEM image (Fig. 7b) also reveals that AlF_3-AIP consisted of nearly

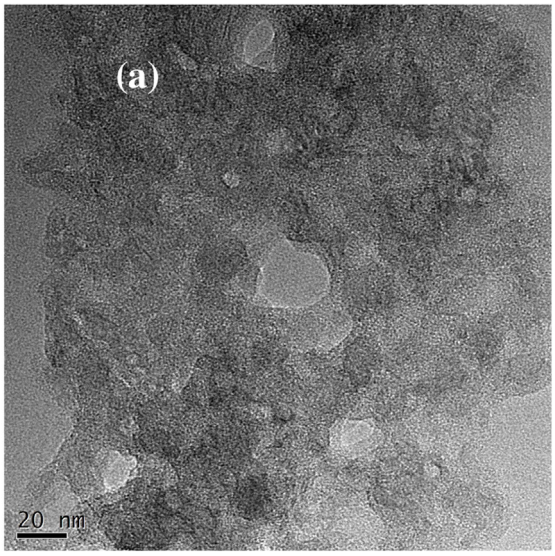

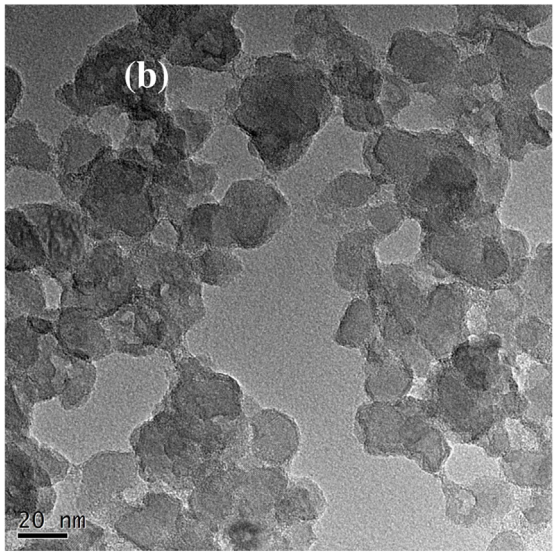

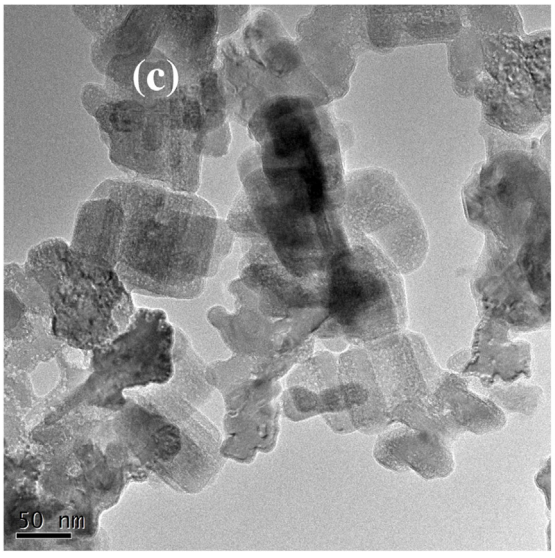

Fig. 7. TEM images of AlF_3 derived from (a) ASO, (b) AlP and (c) ADH.

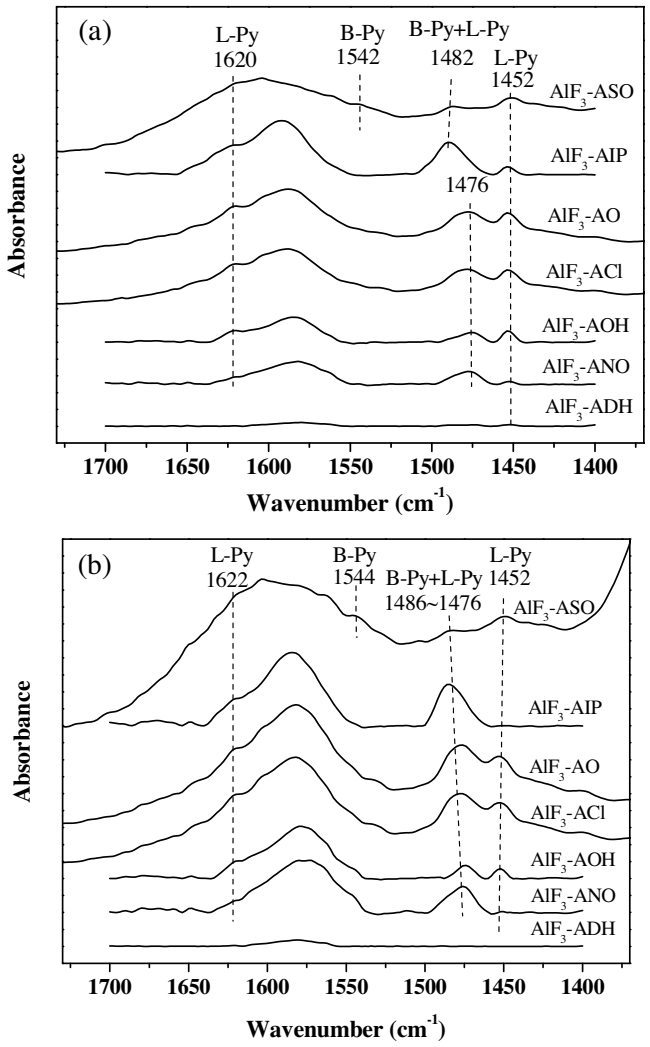

Fig. 8. IR spectrum recorded after pyridine (Py) chemisorption of prepared aluminum fluorides (a) Py desorption at 200 °C and (b) Py desorption at 350 °C. Peaks at (B) are indicative for Brønsted acidity, and peaks at (L) for Lewis acidity.

globular nanoparticles with diameters around 15–35 nm. Large and uniform nanoparticles with quadrilateral-like structure were observed in AlF_3-ADH (Fig. 7c) with diameter around 100 nm, which can be due to the sintering of particles at high thermal-treatment temperature. This explained the low specific surface area of AlF_3-ADH. On the basis of above experimental evidences, it can be concluded that aluminum precursor was vital for the formation of aluminum fluoride in the proposed EGSG route.

3.3. Surface acidic properties of prepared aluminum fluorides

Surface acidic properties of aluminum fluorides derived from different precursors were characterized by FT-IR spectroscopy of pyridine adsorption and temperature-programmed desorption of ammonia (NH_3-TPD). The FT-IR spectra (Fig. 8a) confirmed the presence of Lewis acid sites in all the prepared AlF_3 samples, shown by the vibration bands at 1452 (ν_{19b}) and 1620 (ν_{8a}) cm^{-1} (characteristic for pyridine coordinated on Lewis acid sites) [4,11,13]. However, the intensity of ν_{19b} band was very weak in AlF_3-ADH, indicating the Lewis acid sites were limited in this sample. Furthermore, AlF_3-ASO showed an absorption band at 1542 cm^{-1}, revealing the occurrence of Brønsted acid sites [32,33]. For sulfated metal oxides, the sulfate ion is beneficial to the formation of Brønsted acid sites from the weakening of the O—H bond by the

Table 4
Catalytic activities of prepared aluminum fluorides toward the dehydrofluorination reaction of HFC-134a[a].

Catalyst	HFC-134a conversion (%)	Activity (mmol h^{-1} g^{-1})	Trifluoroethylene selectivity (%)	Lewis acidity amount (μmol g^{-1}) [c]
AlF_3-AOH	24.1	1.229	97.5	47.3
AlF_3-AO	28.3	1.366	99.0	65.9
AlF_3-ACl	17.5	0.999	97.5	61.7
AlF_3-ANO	8.4	0.676	97.1	12.9
AlF_3-ASO	7.4	0.308	99	53.1
AlF_3-AIP	11.9	0.385	97.5	30
AlF_3-ADH	1.7	0.083	99	7.2
AlF_3[b]	9.8	–	98	–

[a] Reaction conditions: T = 400 ◦C, GHSV = 679 h^{-1}, N_2/HFC-134a = 9, amount of catalyst = 5 mL, atmospheric pressure; Results were collected after 20 min reaction time.
[b] From ref. [4].
[c] Estimated from the intensity of band at 1452 cm^{-1} in the FT-IR of pyridine adsorption under thermodesorption at 200 °C.

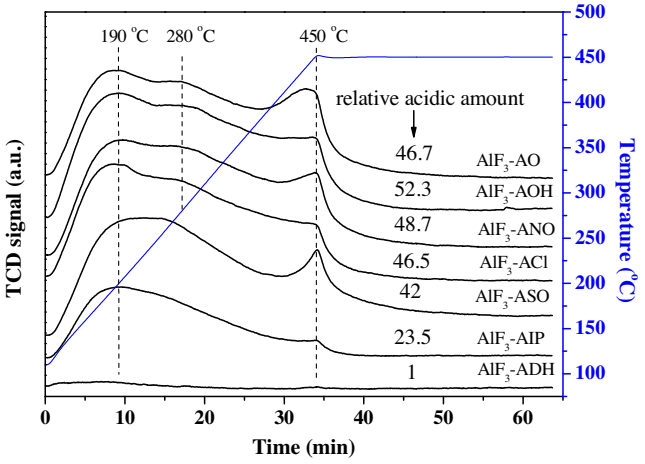

Fig. 9. The NH_3-TPD profiles of various aluminum fluorides.

inductive effect [34]. Thus, it is deduced that the residual sulfate ion can play similar role in AlF_3-ASO. The adsorption band around at 1476–1482 cm^{-1} was also observed in all the prepared AlF_3 samples except AlF_3-ADH, which has been ascribed to both Lewis and Brønsted acid sites [33]. No significant differences were found upon further evacuated at 350 °C (Fig. 8b). The ν_{19b} band was still visible in AlF_3-AOH, AlF_3-AO, AlF_3-ACl and AlF_3-ASO, but the intensity of which decreased significantly in AlF_3-ANO and almost disappeared in AlF_3-AIP. The ratio of the Lewis acidity amounts after pyridine desorption at 350 and 200 °C (estimated from the intensity of ν_{19b} band) was among 0.4 ~ 0.6 for AlF_3-AOH, AlF_3-AO, AlF_3-ACl and AlF_3-ASO, but it decreased to 0.23 for AlF_3-ANO and to 0 for AlF_3-AIP. This result indicates that the Lewis acidic strength of AlF_3-ANO, especially AlF_3-AIP was weaker than those of other prepared HS-AlF_3. It is noted that higher oxygen were incorporated in AlF_3-ANO and AlF_3-AIP than in other AlF_3 samples except AlF_3-ASO which evidently can reduce their Lewis acidic strength. Whereas, considering the presence of sulfur complex, the Lewis acidic strength of AlF_3-ASO may be hardly lessened somehow although the largest amount of oxygen was incorporated in this sample among the prepared AlF_3. Fig. 9 showed the NH_3-TPD for various aluminum fluorides. HS-α-AlF_3 (AlF_3-AOH, AlF_3-AO, AlF_3-ANO and AlF_3-ACl) had three desorption peaks at about 190, 280 and 450 °C, respectively, corresponding to weak, medium and strong acidic sites. The strength of medium acidic sites was weaker in AlF_3-ASO, as indicated by the appearance of desorption peak at lower temperature of 272 °C. Only one remarkable desorption peak at 190 °C can be observed in the AlF_3-AIP, indicating the medium and strong acidic sites were reduced largely in this sample. AlF_3-ADH almost has no acidity due to the absence of ammonia desorption. The relative acidity amounts of different aluminum fluorides were estimated by comparing the peak areas under the curves with that of AlF_3-ADH. The acidity amounts of various aluminum fluorides followed the decreasing order of AlF_3-AOH > AlF_3-ANO > AlF_3-AO > AlF_3-ACl > AlF_3-ASO > AlF_3-AIP » AlF_3-ADH. Interestingly, the acidity amount seems to be high for AlF_3-ANO determined by NH_3-TPD and low determined by FT-IR spectra of pyridine adsorption. Indeed, pyridine is a strong base which is not adsorbed on sites with weak strength but this is not obvious by NH_3-TPD curve in comparison with other fluorides. At this stage of the study, it is difficult to find a rational explanation for this specific point.

3.4. Catalytic dehydrofluorination of HFC-134a over prepared aluminum fluorides

The high specific surface area together with large acidity amount makes this kind of aluminum fluorides a type of attractive materials for catalytic reactions, particularly at elevated temperature. The dehydrofluorination of HFC-134a is an endothermic reaction and the C–F cleavage needs high activation energy, accompanied by high reaction temperature [4]. The catalytic activity of HFC-134a dehydrofluorination over prepared aluminum fluorides was examined at relative low temperature (400 °C) (Table 4). At the same reaction conditions, the conventional AlF_3 prepared by fluorination of γ-Al_2O_3 displayed much low activity with HFC-134a conv. <10%, although the trifluoroethylene selectivity was high (98%). Zhu et al. have reported that the Lewis acid sites of catalyst are the main active centers for the dehydrofluorination of HFC-134a [4]. As a result, the poor activity of conventional AlF_3 is associated with its small specific surface area and low Lewis acid sites. High HFC-134a conversions of 17%–28% with trifluoroethylene selectivity above 97% were achieved on AlF_3-AOH, AlF_3-AO and AlF_3-ACl. Meanwhile, the HFC-134a conversion of AlF_3-AO was approximately three times higher than that of the conventional AlF_3. As shown in Table 4, large amounts of Lewis acid sites were present in above three catalysts, which accounted for their high activity for dehydrofluorination. However, AlF_3-ACl displayed lower activity than AlF_3-AOH. The ratio of the Lewis acidity amounts after pyridine desorption at 350 and 200 °C was 0.43 and 0.53, respectively, for AlF_3-ACl and AlF_3-AOH. This indicated weaker Lewis acidic strength for AlF_3-ACl in comparison with AlF_3-AOH, leading to its relative low activity. According to the results of Py-IR spectra, the low activity of AlF_3-ANO can be ascribed to its weak Lewis acidic strength and small amounts of Lewis acidic sites. Similarly, the weak Lewis acidic strength of AlF_3-AIP leaded to a low catalytic activity. Interestingly, although AlF_3-ASO possessed large Lewis acidity amounts, it exhibited remarkably low activity for dehydrofluorination. Presumably, surface Brønsted acid sites of AlF_3-ASO would inhibit the occurrence of dehydrofluorination reaction. AlF_3-ADH was almost inactive in this reaction, and its activity was even much lower than that of conventional AlF_3. This can be due to the much low surface area with limited acidic sites of AlF_3-ADH. In addition, during HFC-134a dehydrofluorination substantial amounts of HF are formed

which will definitely affect the surface properties of catalyst. As a result, the used AlF_3-AOH catalyst was also characterized. The specific surface area of used AlF_3-AOH reached to 160 $m^2 g^{-1}$, which was larger than that of fresh sample. The EDX analysis showed that the F content was enhanced to 71.2 wt.% in the used AlF_3-AOH, while the O content decreased to 3.6 wt.%. Moreover, minor C (~2.2 wt.%) was also detected. Above results indicate that the AlF_3-AOH was further fluorinated slightly during the reaction, and the fluorination process may improve to some extent its specific surface area. The NH_3-TPD of used AlF_3-AOH (Fig. S7) showed that after reaction the amount of acid sites with medium strength (maximum peak at 286 °C) increased, while the desorption peak (449 °C) corresponding to strong acid sites was reduced. As further fluorination process proceeded over the AlF_3-AOH catalyst during the reaction, surface acidity amount can be enhanced after more F atoms were incorporated into catalyst. Furthermore, considering that surface C content increased after reaction, coke formation may be responsible for decreasing of strong acid sites.

4. Conclusions

In conclusion, we have demonstrated a facile and general preparation of *nano*-aluminum fluorides with diverse phase structures and high specific surface area by a simple ethylene glycol mediated sol-gel process. Aluminum precursor is crucial for the physical–chemical properties of the resulting fluoride. Using low-cost inorganic salt hydrates and oxides as precursors, the resulting AlF_3 has α phase structure, high specific surface area (up to 170 $m^2 g^{-1}$) and mesopores even after high-temperature calcination. Amorphous AlF_3 with high specific surface area of 191 $m^2 g^{-1}$ was prepared using $Al_2(SO_4)_3 \cdot 18H_2O$ as precursors. The resulting AlF_3 derived from aluminum isopropoxide exhibited the pyrochlore phase with specific surface area ~100 $m^2 g^{-1}$ under the same preparation conditions. Amorphous and pyrochlore phase AlF_3 possessed both the Lewis and Brønsted acid sites. Furthermore, the large surface area and strong Lewis acidity make the obtained HS-α-AlF_3 derived from oxides a highly active catalyst for HFC-134a dehydrofluorination. Most importantly, this facile synthesis strategy can be easily extended to design other metal fluoride catalysts.

Acknowledgment

We are grateful to be supported in part by industrial research project of Shaanxi Province (No. 2014K10-11).

Appendix A. Supplementary data

The surface elemental compositions of various α-AlF_3; XRD patterns of various gels and AlF_3 obtained from the precipitation method in ethanol; In-situ FTIR spectra of gel-AOH; SEM images of various HS-α-AlF_3; FT-IR of AlF_3 derived from ASO, AIP and ADH, gel-AIP and AlF_3-AIP; NH_3-TPD of used AlF_3-AOH.

Supplementary data associated with this article can be found, in the online version, at http://dx.doi.org/10.1016/j.apcatb.2016.12.064.

References

[1] (a) G.J.M. Velders, A.R. Ravishankara, M.K. Miller, M.J. Molina, J. Alcamo, J.S. Daniel, D.W. Fahey, S.A. Montzka, S. Reimann, Science 335 (2012) 922–923; (b) X.K. Fang, G.J.M. Velders, A.R. Ravishankara, M.J. Molina, J.X. Hu, R.G. Prinn, Environ. Sci. Technol. 50 (2016) 2027–2034.
[2] (a) S.V. Renssen, Nature 2 (2012) 143–144; (b) S. Papasavva, D.J. Luecken, R.L. Waterland, K.N. Taddonio, S.O. Andersen, Environ. Sci. Technol. 44 (2010) 343–348.
[3] K. Teinz, S.R. Manuel, B.B. Chen, A. Pigamo, N. Doucet, E. Kemnitz, Appl. Catal. B 165 (2015) 200–208.
[4] W.Z. Jia, M. Liu, X.W. Lang, C. Hu, J.H. Li, Z.R. Zhu, Catal. Sci. Technol. 5 (2015) 3103–3107.
[5] F. Wang, W.X. Zhang, Y. Liang, Y.J. Wang, J.Q. Lu, M.F. Luo, Chem. Res. Chin. Univ. 31 (2015) 1003–1006.
[6] M.K. Whittlesey, E. Peris, ACS Catal. 4 (2014) 3152–3159.
[7] E. Kemnitz, Catal. Sci. Technol. 5 (2015) 786–806.
[8] T. Skapin, G. Tavčar, A. Benčan, Z. Mazej, J. Fluor. Chem. 130 (2009) 1086–1092.
[9] K. Teinz, S. Wuttke, F. Börno, J. Eicher, E. Kemnitz, J. Catal. 282 (2011) 175–182.
[10] E. Kemnitz, U. Groβ, S. Rüdiger, C.S. Shekar, Angew. Chem. Int. Ed. 42 (2003) 4251–4254.
[11] D. Dambournet, G. Eltanamy, A. Vimont, J.C. Lavalley, J. Goupil, A. Demourgues, E. Durand, J. Majimel, S. Rudiger, E. Kemnitz, J.M. Winfield, A. Tressaud, Chem. Eur. J. 14 (2008) 6205–6212.
[12] J.L. Delattre, P.J. Chupas, C.P. Grey, A.M. Stacy, J. Am. Chem. Soc. 123 (2001) 5364–5365.
[13] W.Z. Jia, J.Q. Lu, P. Chen, Y.J. Wang, M.F. Luo, J. Mater. Chem. 21 (2011) 8987–8990.
[14] D. Dambournet, A. Demourgues, C. Martineau, E. Durand, J. Majimel, A. Vimont, H. Leclerc, J.C. Lavalley, M. Daturi, C. Legein, J.Y. Buzaré, F. Fayone, A. Tressaud, J. Mater. Chem. 18 (2008) 2483–2492.
[15] D. Dambournet, A. Demourgues, C. Martineau, J. Majimel, M. Feist, C. Legein, J.Y. Buzaré, F. Fayon, A. Tressaud, J. Phys. Chem. C 112 (2008) 12374–12380.
[16] G. Scholz, R. König, J. Petersen, B. Angelow, I. Dörfel, E. Kemnitz, Chem. Mater. 20 (2008) 5406–5413.
[17] C.L. Bailey, S. Mukhopadhyay, A. Wander, B.G. Searle, N.M. Harrison, J. Phys. Chem. C 113 (2009) 4976–4983.
[18] C. Alonso, A. Morato, F. Medina, Y. Cesteros, P. Salagre, J.E. Sueiras, Appl. Catal. B 40 (2003) 259–269.
[19] M.B. González, A.Y. Wu, P.M. Vilarinho, Chem. Mater. 18 (2006) 1737–1744.
[20] G. Frenzer, W.F. Maier, Annu. Rev. Mater. Res. 36 (2006) 281–331.
[21] P. Schmitt, N. Brem, S. Schunk, C. Feldmann, Adv. Funct. Mater. 21 (2011) 3037–3046.
[22] M. Estruga, F. Meng, L.S. Li, L.Y. Chen, X.C. Li, S. Jin, J. Mater. Chem. 22 (2012) 20991–20997.
[23] C. Alonso, A. Morato, F. Medina, F. Guirado, Y. Cesteros, P. Salagre, J.E. Sueiras, Chem. Mater. 12 (2000) 1148–1155.
[24] C. Stosiek, G. Scholz, G. Eltanany, R. Bertram, E. Kemnitz, Chem. Mater. 20 (2008) 5687–5697.
[25] (a) Y.Z. Xi, R.J. Davis, Inorg. Chem. 49 (2010) 3888–3895; (b) A. Kasai, S. Fujihara, Inorg. Chem. 45 (2006) 415–418.
[26] C. Stosiek, G. Scholz, S.L.M. Schroeder, E. Kemnitz, Chem. Mater. 22 (2010) 2347–2356.
[27] Y.M. Lu, H. Li, J. He, Y.X. Liu, Z.B. Wu, D.Y. Hu, S. Yang, RSC Adv. 6 (2016) 12782–12787.
[28] F. Frouri, S. Célérier, P. Ayrault, F. Richard, Appl. Catal. B 168–169 (2015) 515–523.
[29] A. Štefančič, D. Primc, G. Tavčara, T. Skapin, Dalton Trans. 44 (2015) 20609–20617.
[30] D. Dambournet, A. Demourgues, C. Martineau, E. Durand, J. Majimel, C. Legein, J.Y. Buzaré, F. Fayon, A. Vimont, H. Leclerc, A. Tressaud, Chem. Mater. 20 (2008) 7095–7106.
[31] A. Patel, G. Coudurier, N. Essayem, J.C. Védrine, J. Chem. Soc. Faraday Trans. 93 (1997) 347–353.
[32] P.T. Patil, A. Dimitrov, H. Kirmse, W. Neumann, E. Kemnitz, Appl. Catal. B 78 (2008) 80–91.
[33] O. Machynskyy, E. Kemnitz, Z. Karpiński, ChemCatChem 6 (2014) 592–602.
[34] J.R. Sohn, S.H. Lee, J.S. Lim, Catal. Today 116 (2006) 143–150.